Composite Luminosity Functions of the Sloan Digital Sky Survey Cut & Enhance Galaxy Cluster Catalog

Tomotsugu GOTO[1,2,3], Sadanori OKAMURA[4], Timothy A. MCKAY[5],

James ANNIS[6], Neta A. BAHCALL[7], Mariangela BERNARDI[2],

J. BRINKMANN[8], Percy L. GOMEZ[2], Sarah HANSEN[5],

Rita S. J. KIM[9], Maki SEKIGUCHI[1] and Ravi K. SHETH[10]

[1] *Institute for Cosmic Ray Research, University of Tokyo,*

Kashiwanoha, Kashiwa, Chiba 277-0882, Japan

[2] *Department of Physics, Carnegie Mellon University,*

5000 Forbes Avenue, Pittsburgh, PA 15213-3890, USA

[3] *tomo@cmu.edu*

[4] *Department of Astronomy and Research Center for the Early Universe,*

School of Science, University of Tokyo, Tokyo 113-0033, Japan

[5] *University of Michigan, Department of Physics,*

500 East University, Ann Arbor, MI 48109, USA

[6] *Fermi National Accelerator Laboratory, P.O. Box 500, Batavia, IL 60510, USA*

[7] *Princeton University Observatory, Princeton, NJ 08544, USA*

[8] *Apache Point Observatory,*

2001 Apache Point Road, P.O. Box 59, Sunspot, NM 88349-0059, USA

[9] *Department of Physics and Astronomy, The Johns Hopkins University,*

3400 North Charles Street, Baltimore, MD 21218-2686, USA

[10] *Department of Physics and Astronomy University of Pittsburgh*

3941 O'Hara Street Pittsburgh, PA 15260

Abstract

We present here results on the composite luminosity functions of galaxies in the clusters of galaxies selected from the Cut and Enhance cluster catalog (CE; Goto et al. 2001) of the Sloan Digital Sky Survey (SDSS; York et al. 2000). We construct the composite luminosity function in the five SDSS bands, u^*, g^*, r^*, i^* and z^*, using 204 CE clusters ranging from $z=0.02$ to $z=0.25$. Background and foreground galaxies are subtracted from the luminosity function using an annular region around clusters to take large scale, galaxy number count variances into consideration. The wide coverage of SDSS data enabled to estimate background and foreground locally. A luminosity function of each cluster is weighted according to richness and number

of contributing galaxies to construct the composite luminosity function. Taking advantage of accurate photometry of SDSS, we use photometric redshifts to construct composite luminosity functions and thus study the large number of clusters. The robustness of the weighting scheme was tested using Monte Carlo simulation. The best fit Schechter parameters are (M^*,α)=(-21.61±0.26, -1.40±0.11),(-22.01±0.11, -1.00±0.06),(-22.21±0.05, -0.85±0.03), (-22.31±0.08, -0.70±0.05) and (-21.36±0.06, -0.58±0.04) in u^*, g^*, r^*, i^* and z^*, respectively. We find the slope of composite LFs become flatter toward redder color band. Comparing with field LFs of SDSS (Blanton et al. 2001), cluster LFs have brighter characteristic magnitude and flatter slopes in g^*, r^*, i^* and z^* bands. These results are consistent with the hypothesis that the cluster LF has two distinct underlying populations *i.e.* the bright end of the LF is dominated by bright early types that follow a gaussian–like luminosity distribution, while the faint–end of the cluster LF is a steep power–law like function dominated by star–forming (bluer) galaxies. We also study the composite luminosity functions for early–type and late–type galaxies using profile fits, a concentration parameter and $u^* - r^*$ color to classify galaxy morphology. The strong dependence of LF on galaxy morphology is found. The faint end slope of the LF is always flatter for early–type galaxies than late–type regardless of passband and methodology. These results are consistent with the hypothesis that the cluster region are dominated by bright elliptical galaxies. This work also provide a good low–redshift benchmark for on–going multi-color photometric studies of high redshift clusters of galaxies using 4-8m class telescopes.

Key words: galaxies: clusters: general — galaxies: luminosity function, mass function

1. Introduction

The luminosity function (LF) of galaxies within clusters of galaxies is a key tool for understanding the role of environment on galaxy formation and evolution. The shape of the cluster LF as a function of galaxy colors and morphologies, as well as a function of cluster radius or local density, can provide strong observational constraints on theories of galaxy formation. For example, Springel et al. (2001) recently showed that semi–analytical models of hierarchical structure formation could now explain both the shape of the composite cluster LF (B–band LF of Trentham et al. 1998) and the morphology–radius relationship of Whitmore et al. (1993) using just a simple prescription for the properties of galaxies in clusters based on their merger and cooling rates (see also Okamoto & Nagashima 2001). Empirically, there is also growing evidence for a correlation between the shape of the cluster LF and the underlying cluster properties. Phillipps et al. (1998) and Driver et al. (1998) show that more evolved clusters,

2

based on either their density profile or the presence of a cD galaxy, have flatter faint–end slopes which they attribute to the disruption of faint galaxies in the cores of such evolved systems (see the earlier theoretical work on galaxy cannibalism by Hausman & Ostriker 1978). In summary, the LF of galaxies in clusters as a function of both the galaxy and cluster properties is a powerful observational test for theories of galaxy formation and evolution. The reader is referred to the seminal review by Binggeli, Sandage & Tammann (1988) which is still relevant today.

In this paper, we present an analysis of the composite cluster LF based on the commissioning data of the Sloan Digital Sky Survey (SDSS; see Gunn et al. 1998, York et al. 2000, Stoughton et al. 2002). This analysis has several key advantages over previous studies of the composite cluster LF, including accurate multi–color CCD photometry for all galaxies (in optical passbands u^*,g^*,r^*,i^* and z^*; Fukugita et al. 1996), large aerial coverage thus enabling us to make a local correction for the projected field LF and finally, the availability of several objectively–measured galaxy properties like morphology. Furthermore, we have selected our clusters from the SDSS Cut & Enhance (CE) cluster catalog of Goto et al. (2002) which has two major benefits over previous cluster samples used for LF studies. First, the CE catalog was objectively constructed using the latest cluster–finding algorithms, and therefore has a well-determined selection function (see Goto et al. 2002). Secondly, CE has obtained an accurate photometric redshift for each cluster based on the observed color of the E/S0 ridge–line using the method described in Annis et al. (2002). The error on this cluster photometric redshift is only $\delta z = 0.015$ for $z < 0.3$ clusters (see Fig. 14 of Goto et al. 2002) and, as we will show herein, is accurate enough to allow us to determine the composite LF for a large sample of CE clusters without the need for spectroscopic redshifts. Thus our analysis of the composite cluster LF is based on one of the largest sample of clusters to date.

We present this work now to provide a low–redshift benchmark for on–going multi-color photometric studies of high redshift clusters of galaxies. With the advent of large–area CCD imagers on large telescopes, the number of distant clusters with such data will increase rapidly over the next few years, e.g. Kodama et al. (2001) recently presented large–area multi–color CCD photometry for distant cluster A851 ($z = 0.41$) using Suprime-Cam on the Subaru Telescope. Gladders et al. (2000) search distant clusters over 100 deg² of CCD data. This paper is organized as follows: In Sect. 2, we describe the methods used in constructing the composite LF of CE clusters and show our results as a function of passband and morphology. In Sect. 3, we test the robustness of the analysis, and in Sect. 4, we summarize our work. Throughout this paper, we have used $h_0=0.7$, $\Omega_M=0.3$ and $\Omega_\Lambda=0.7$.

2. SDSS Data

In this section, we outline the data used in this paper. The photometric data used herein was taken from the SDSS commissioning data as discussed in York et al. (2000). Our analysis focuses on the 150 deg² contiguous area made up from the overlap of SDSS photometric runs

3

752 & 756 *i.e.* 145.1<RA<236.0 degrees and -1.25<DEC<+1.25 degrees. This is a subset of the SDSS Early Data Release as discussed in Stoughton et al. (2002) and similar to the data used by Scranton et al. (2001) for studying the angular clustering of SDSS galaxies. This photometric data reaches 5σ detection limits for point sources of 22.3, 23.3, 23.1, 22.3 and 20.8 magnitudes in the u^*, g^*, r^*, i^* and z^* passbands respectively (for an airmass of 1.4 and $1''$ seeing)[1] The photometric uniformity of the data across the whole area is less than 3% (see Hogg et al. 2002 and Smith et al. 2002 for photometric calibration), while the star–galaxy separation is robust to $r^* \simeq 21.0$ (see Scranton et al. 2001). This is significantly better than previous photographic surveys, which suffer from larger plate–to–plate photometric fluctuations and a lower dynamic range (see Lumsden et al. 1997 for the problems associated with photographic studies of the cluster composite LF). For each galaxy, we have used the model magnitude computed by the PHOTO data analysis pipeline, which has been shown by Lupton et al. (2001, 2002) and Stoughton et al. (2002) to be the optimal magnitude for faint SDSS galaxies. It is also close to a total magnitude for the fainter SDSS galaxies. For a full discussion of the photometric data, and the galaxy parameters derived from that data, we refer the reader to Lupton et al. (2001, 2002) and Stoughton et al. (2002).

The clusters used herein were drawn from the large sample of CE clusters presented in Goto et al. (2002), which were selected over the same photometric runs of 752 & 756. We have only selected the richer systems which were determined by the number of galaxies brighter than -18th magnitiude, (N_{-18}). The CE clusters used here satisfy the following conditions.

1, Number of galaxies brighter than -18th magnitude in r^* band (N_{-18}) > 20.

2, 0.02< z <0.25

The condition 1 is used to select richer systems. N_{-18} is defined as a number of galaxies brighter than -18th magnitude in r^* band after subtracting the backgound using the method described in Sect. 3 to construct composite LFs. Galaxies within 0.75 Mpc from a cluster center are used. The condition 1 is used to avoid letting the small groups with only a few very bright galaxies dominate the composite LFs in the weighting scheme. (The weighting scheme is explained in detail in Sect. 3). Even though we select N_{-18} >20 as a criteria to select our clusters, we show in Sect. 4 that our composite LFs are not affected by this richness criteria. Since the high redshift clusters ($z \sim 0.3$) are not imaged to the fainter galaxies, we restrict our clusters in the range 0.02< z <0.25. In total, 204 clusters satisfy these criteria.

---

[1] The SDSS filter system defined by Fukugita et al. (1996) is denoted u', g', r', i' and z'. The photometry, however, obtained at this early stage of SDSS is denoted u^*, g^*, r^*, i^* and z^* to stress the preliminary nature of the calibration.

3. Analysis and Results

3.1. *Construction of the Composite Cluster LF*

We discuss here the construction of the composite luminosity function of galaxies within the subsample of the CE clusters discussed above. The first critical step in such an analysis is the subtraction of background and foreground contamination. Ideally, one would wish to do this via spectroscopic observations but since the CE cluster catalog contains ∼2000 galaxies in the region used, it is not feasible to observe all clusters spectroscopically. Therefore, we must make a statistical correction based on the expected contamination from projected field galaxies. One of the main advantages of the SDSS data is that such a correction can be estimated locally – free from galaxy number count variances due to large scale structure – for each cluster since we possess all the photometric data, to the same depth and in the same filter set, well outside of the cluster. Indeed such local background subtraction was thought to be ideal in previous works, but was not possible due to the small coverage of the sky.

For the composite cluster LF, we only use galaxies within 0.75 Mpc of the cluster centroid. This radius has been determined empirically not to lose statistics by using too small a radius, and not to lose the contrast of clusters against the background by using too large a radius. Foreground and background contamination is corrected for using an annulus around each cluster with an inner radius of 1.5 Mpc and an outer radius of 1.68 Mpc. These radii represent a compromise between having as large an aperture as possible to avoid removing legitimate cluster galaxies, while still providing an accurate estimate of the local projected field population. Since the background/foreground galaxies are themselves highly clustered, it is important to obtain as local an estimate as possible. The photometric redshift of each cluster was used to convert these metric apertures into angular apertures. The center of each cluster was taken from the CE catalog, and was estimated from the position of the peak in the enhanced density map of Goto et al. (2002). The cluster centroids are expected to be determined with an accuracy better than ∼40 arcsec through Monte Carlo simulation. When an annulus touches the boundary of the SDSS data, we correct for contamination using the number–magnitude relationship of the whole data set instead (this only affected a few of the clusters used herein).

Since each sample cluster has different redshift, each cluster reaches SDSS apparent magnitude limit at different absolute magnitudes. Also, because they have various richnesses, the number of galaxies in each cluster is different. To take these different degrees of completeness into account, we follow the methodology of Colless (1989) to construct the composite cluster LF. The individual cluster LFs are weighted according to the cluster richness and the number of clusters which contribute to a given bin. This is written as,

$$N_{cj} = \frac{m_j}{N_{c0}} \sum_i \frac{N_{ij}}{N_{i0}}, \tag{1}$$

where N_{cj} is the number of galaxies in the jth bin of the composite LF, N_{ij} is the number in the

5

jth bin of the ith cluster LF, N_{i0} is the normalization of the ith cluster LF, and is measured to be the field-corrected number of galaxies brighter than $M_{r*} = -18$, m_j is the number of clusters contributing the jth bin and finally, $N_{c0} = \sum_i N_{i0}$. The formal errors on the composite LF are computed using,

$$\delta N_{cj} = \frac{N_{c0}}{m_j} \left[\sum_i \left(\frac{\delta N_{ij}}{N_{i0}} \right)^2 \right]^{1/2} \tag{2}$$

where δN_{cj} and δN_{ij} are the errors on the jth bin for the composite and the ith cluster, respectively. In this way we can take into account the different degrees of completeness.

Like other authors, we have discarded the Brightest Cluster Galaxy (BCG) within 0.75 Mpc of the cluster centroid when constructing the composite LF since such BCGs tend not to follow the cluster LF. We only use SDSS galaxies brighter than r^*=21.0 since this is the limit of the SDSS star-galaxy separation (Scranton et al. 2001; Lupton et al. 2001, 2002). This magnitude limit and weighting scheme combined with our cosmology enable us to dig LF down to M_{r*}=-17.5 . When converting apparent to absolute magnitudes, we assumed a k-correction for the early–type galaxy given by Fukugita et al. (1995).

In Fig. 1, we show the composite LF of the subset of CE clusters discussed above. We present one composite LF for each of the five SDSS passbands. We also present in Table 1 the best fit parameters from a joint fit of a Schechter function to these data. For comparison, we also show the field values as derived by Blanton et al. (2001) (corrected for h_0=0.7). In Fig. 1, field LFs normalized to cluster LFs are shown with dotted lines. As expected, the M^* for our cluster LFs is significantly brighter (by $1 \sim 1.5$ magnitudes depending on the bands) than those seen for the field LFs in all five bands. Furthermore, the faint end slopes (α) of the cluster composite LFs are much flatter that those seen for the field LFs. This is especially noticeable for the redder passbands (i^* and z^*) while the slope of the cluster LF systematically flattens from the u^* passband to the z^* passband.

These results are consistent with the hypothesis that the cluster LF has two distinct underlying populations $i.e.$ the bright end of the LF is dominated by bright early types that follow a Gaussian–like luminosity distribution, while the faint–end of the cluster LF is a steep power–law–like function dominated by star–forming (bluer) galaxies (see Binggeli et al. 1988 for this original hypothesis, while the recent work of Adami et al. 2000, Rakos et al. 2000 and Dressler et al. 1999 support this idea. Particularly, Boyce et al.(2001) showed LF of Abell 868 is made up of three different populations of galaxies; luminous red and two fainter blue populations). The idea is illustrated by the fact that the cluster LFs in the redder passbands, which are presumably dominated by the old stellar populations of the early types, have much brighter M^*s and significantly shallower slopes than those measured in the bluer passbands. Those results can also be interpreted as showing that bright elliptical galaxies are more populated in dense regions like inside of clusters. They are consistent with the morphology–density relation advocated by Dressler et al. (1980, 1997).

3.2. The Composite Cluster LF as a Function of Morphology

One of the key aspects of the SDSS photometric data is the opportunity to statistically study the distribution of galaxies as a function of their morphology. In this Section, we discuss the composite cluster LF as a function of morphology using three complementary methods for determining the morphological type of each galaxy. These include: *i)* The best fit de Vaucouleur or exponential model profile; *ii)* The inverse of concentration index and *iii)* the $u^* - r^*$ color of the galaxies. We present all three methods since at present it is unclear which method is the most successful at separating the different morphological galaxy types. Also, each method suffers from different levels of contamination and the differences in the methods can be used to gauge the possible systematic uncertainties in the morphological classifications. We discuss the three methods used in detail below.

The first method we consider here is using the de Vaucouleur and exponential model fits of the galaxy light profiles measured by SDSS photometric pipeline ($PHOTO$ see Lupton et al. 2002) to broadly separate galaxies into late and early–type. If the likelihood of a de Vaucouleur model fit to the data is higher than the likelihood of an exponential model fit, the galaxy is called a late–type, and vice versa. Galaxies that have the same likelihoods for both model fits are discarded. In Fig. 2, we present the composite cluster LF of late–type and early–type galaxies (as defined using the model fits above) for all five SDSS passbands. In Table 2, we present the best fit Schechter function parameters to these data and show the fits in Fig. 2.

The second method uses the inverse of the concentration index, which is defined as $C = r_{50}/r_{90}$, where r_{50} is the radius that contains 50% of the Petrosian flux and r_{90} is the radius that contains 90% of the Petrosian flux (see Lupton et al. 2002). Both these parameters are measured by the SDSS PHOTO analysis pipeline for each galaxy. The concentration parameter used here (C) is just the inverse of the commonly used concentration parameter and thus early–type galaxies have a lower C parameter than late–type galaxies. The correlation of C with visually–classified morphologies has been studied in detail by Shimasaku et al. (2001) and Strateva et al. (2001). They found that galaxies with $C <0.4$ are regarded as early–type galaxies, while galaxies with $C \geq 0.4$ are regarded as late–type galaxies. Therefore, in Fig. 3, we show the composite cluster LF of late–type and early–type galaxies as defined using this second method for all five SDSS passbands. In Table 3, we present the best fit Schechter function parameters to these data.

The third method used herein for morphological classification was to use the observed $u^* - r^*$ color of the galaxy which has been proposed by Strateva et al. (2001). Using the fact that k-correction for $u^* - r^*$ is almost constant until $z=0.4$, they showed that galaxies shows a clear bimodal distribution in their $u^* - r^*$ color and $u^* - r^*=2.2$ serves as a good classifier of morphology until $z \sim 0.4$ by correlating $u^* - r^*$ classification with visual classifications. Therefore, we have classified galaxies with $u^* - r^* <2.2$ as early–type and galaxies with $u^* - r^* \geq 2.2$ as late–type. Fig. 4 shows the composite cluster LF for both types of galaxies

7

along with their best fit Schechter functions (in all five passbands). The best fit Schechter parameters are summarized in Table 4.

As expected, there are noticeable differences in these three morphological classifications as portrayed by the differences in their composite LFs (see Figs. 2, 3 and 4). However, it is worth stressing here the similarities between the methods. For example, the faint end slope of the LF is always shallower for early–type galaxies than late–type regardless of passband and methodology. Also, the faint end slope for early–type galaxies decreases steadily toward the redder passbands, while the faint–end slope for the late–type galaxies is nearly always above -1 and consistent (or steeper) than the field LF in most passbands. These observations are again qualitatively in agreement with the hypothesis that the bright end of the cluster LF is dominated by bright, old early–types, while the faint–end of the cluster LF represents late–type galaxies maybe in greater numbers than the average field. This model is in agreement with hierarchical models of structure formation and the model for the tidal disruption of dwarf galaxies by the dominant early types.

4. Discussion

In this Section, we discuss various tests we have performed on our measurement and results.

4.1. Monte Carlo Simulations

To test the robustness of our methods, we have performed Monte Carlo simulations which involved adding artificial clusters to the SDSS data and computing their composite LF using the same algorithms and software as used on the real data. Our model for the artificial clusters was constructed using the SDSS data on Abell 1577 (at $z \sim 0.14$, Richness~ 1). We used the method described in Goto et al. (2002) to make artificial clusters. The radial profile for the artificial clusters was taken to be a King profile (Ichikawa 1986) with a concentration index of 1.5 and a cut–off radius of 1.4 Mpc, which is the size of Abell 1577 (Struble & Rood 1987). The color–magnitude distributions for the artificial clusters were set to be the observed, field–corrected, color–magnitude distributions of Abell 1577 binned into 0.2 magnitude bins in both color and magnitude. From this model, we then constructed artificial clusters as a function of redshift and overall richness. For redshift, we created clusters at z=0.2, 0.3, 0.4 and 0.5 ensuring that we properly accounted for the cosmological effects $i.e.$ the clusters became smaller, redder and dimmer with redshift. We used the k–corrections for an early type spectrum. For richness, we change the number of galaxies within each cluster randomly between 10 and 50. For each redshift, we create 100 clusters (400 clusters in total). The galaxies within these artificial cluster were distributed randomly in accordance with the radial and color–magnitude distributions discussed above. We made no attempt to simulate the density–morphology relation nor the luminosity segregation in clusters.

8

The artificial clusters were randomly distributed within the real SDSS imaging data and we constructed a composite LF for these clusters using exactly the same software as for the real clusters. Since the artificial clusters are all made from the same luminosity distribution, the composite LF should therefore look very similar in shape as the original input LF. Fig. 5 shows the result of our Monte Carlo simulations. The histogram shows the original absolute magnitude distribution of Abell 1577 after the field correction, while the symbols show the composite luminosity functions we constructed as a function of input redshift.

4.2. Check of Photometric Redshifts

One of the most innovative parts of this analysis is the use of photometric redshifts to determine the composite luminosity function of clusters. As demonstrated in Goto et al. (2002), the accuracy of photometric redshift is excellent ($\delta z = \pm 0.015$ for $z < 0.3$) and this method will certainly be used in the near future as the number of clusters with a photometric redshift will increase rapidly, far quicker than the number of clusters with a spectroscopically confirmed redshift.

To justify our use of photometric redshifts, since all previous composite cluster LF's used spectroscopic redshifts, we have constructed here a composite LF using only the clusters with spectroscopically confirmed redshifts. We derived our spectroscopic redshift for CE clusters by matching the SDSS spectroscopic galaxy data with our CE clusters. This was achieved by looking in the SDSS spectroscopic galaxy sample for any galaxies within the CE cluster radius and within $\delta z = \pm 0.01$ of the photometric redshift of the cluster. The radius used here is from Goto et al. (2002). If multiple galaxies satisfy this criteria, the closest spectroscopic redshift to the photometric redshift is adopted. The number of clusters with spectroscopic redshifts is 75 out of 204 at the date of this writing.

The results of this test are shown in Fig. 1, (in the bottom right–hand panel). Also the parameters for the best fit Schechter functions are shown in Table 1. and referred to as r^*(spec). We only performed this test for the r^* passband. The slope and characteristic magnitude of the best fit Schechter function for the spectroscopically determined LF is in good agreement with that derived using photometric redshifts. As seen in Table 1, both M_r^* and the slope agree within the error. This test shows that we can truly construct composite LFs using photometric redshift of clusters.

4.3. Test of Cluster Centroids

One key aspect of measuring the composite cluster LF is the choice of cluster centroid. To test the effect of different cluster centroids on the composite LF, we constructed a composite cluster LF using the position of Brightest Cluster Galaxies (BCGs) as a centroid instead of the peak in the enhanced density map as discussed in Goto et al. (2002). The BCGs are determined to be the brightest galaxy among the galaxies fainter than -24th magnitude within 0.75 Mpc. Galaxies brighter than -24th magnitude are regarded as foreground galaxies. The mean offset

9

between the BCG position and the centroid previously used is 1.02 arcmin. Table 6 shows the parameters of the best fit Schechter functions to the five SDSS passbands which should be compared to the values obtained using the optical centroid given in Table 1. In all five bands, the characteristic magnitudes and slopes agree very well within the error. This test shows our composite LFs are not dependent on center determination.

4.4. Test of Background Subtraction

Since we construct composite LFs from 2-dimensional, projected sky image, subtraction of fore/background galaxies plays important role in this work. We test here the effect of making a global background subtraction for all clusters instead of the local background subtraction discussed above. We use the number magnitude relation of all the galaxies in the entire 150 deg^2 region as global background. Table 7 shows the best fit Schechter parameters of composite LFs constructed using global background subtraction. Comparing with Table 1, again, every Schechter parameters agree very well within 1 σ. Although we use annuli around clusters to subtract the background to avoid the large scale structure disturbing the measurement of composite LFs, this test shows that our composite LFs are not dependent on background subtraction. Valotto et al. (2001) showed that a statistical background subtraction can not re-produce composite LFs using a mock galaxy catalog constructed from a large N-body simulation. Our result, however, combined with the fact that we derive the same LF as input through Monte Carlos simulation (in Sect. 4.1), supports that our composite LFs are not subject to background subtraction.

4.5. Test of Cluster Richness

Another aspect we were concerned about was our choice of cluster richness criteria. To test this, we construct composite LFs of different subsample with $N_{-18} > 20$ and $N_{-18} > 40$ in Table 8. N_{-18} here is defined as the number of galaxies brighter than -18th magnitude after subtracting the background in the way we construct composite LFs. $N_{-18} > 20$ is used to construct composite LFs in section 3. In Table 8, even though M^* is slightly brighter and the slope is slightly steeper for the richer sample, they agree within 1 σ. The steepening of the slopes can be interpreted as the bias in selecting richer systems using N_{-18}, *i.e.* Clusters with steeper tails tend to have larger value of N_{-18}. This, however, confirms that our composite LFs are not dependent on richness criteria we choose.

4.6. Comparison with Other LFs

As the final test of our composite cluster LF, we compare here our composite LFs with previous works. First, we must be careful to match the different cosmologies used by the various authors as well as the different photometric passbands. To facilitate such a comparison therefore, we present in Table 9, the best fit Schechter function parameters for our composite LF but calculated for each author's cosmology and passband using the color corrections of

10

Fukugita et al. (1995) and Lumsden et al. (1992).

In the case of the three b_j photographic surveys of Colless (1989), Valotto et al. (1997) and Lumsden et al. (1997), we find a significantly brighter M^* than these studies as well as a much shallower slope. We also tried to fit a Schechter function using their α value for slope, but M^*s become even brighter. The fits are not good when fixed α's are used.

Lugger (1989) found M_R=-22.81±0.13 and α=-1.21±0.09 by re–analyzing nine clusters presented in Lugger (1986). The slope is steeper and M^* is slightly brighter than our results. When we fix the slope with her value at α=-1.21, the two LFs agree well.

Garilli et al. (1999) studied 65 Abell and X-ray selected samples of galaxies in the magnitude range of -23.0< M_r <-17.5 and found that M_r^*=-22.16±0.15 and α=-0.95±0.07 (in isophotal magnitudes). This slope is steeper than ours. A possible difference with ours is that they used the color condition to select cluster galaxies. M^* is in agreement with our results within the error. We also tried to fit a Schechter function with a fixed value of α=0.84. M^* becomes brighter by 0.18 magnitude although the fit was poor.

Paolillo et al. (2000) studied composite LF of 39 Abell clusters using the digitized POSS-II plates. They obtained M^*=-22.17±0.16 in r. The slope is α=-1.11$^{+0.07}_{-0.09}$. Although the slope differs significantly, M^* agrees well comparing with our composite LF.

Yagi et al. (2002a,b) observed 10 nearby clusters with their Mosaic CCD camera to derive composite LF. Their best fit Schechter parameters are M^*=-21.1±0.2 and α=-1.49±0.05 in R. They also studied type–specific LF using exponential and $r^{1/4}$ profile fit to classify galaxy types. They derived M^*=-21.1 and α=-1.49 for exponential galaxies and M^*=-21.2 and α=-1.08 for $r^{1/4}$ galaxies. Considering that they derived composite LFs using the data taken with different instruments analyzed in a different way, it is reassuring that they reached the same conclusion as our results derived in Sect. 3.2. $i.e.$ exponential galaxies have the steeper faint end tail than $r^{1/4}$ galaxies while their M^* are almost the same.

On the disagreement of our LFs with previous works, various differences in measuring composite LFs may be the reason. The possible sources of differences are different way of weighting, different way of background subtraction and different depth of the luminosity function fitted. The sample clusters themselves should have, to some extent, different richness distributions. For M^*, although we try to transform our magnitude into their magnitude, the color conversion between SDSS bands and others might not be accurate enough. Thus, the difference with the previous works is not necessary the mistake in analysis but rather it represents different way of analysis. Throughout our analysis in Sect. 3 we carefully use exactly the same way to construct the composite LFs. We thus keep our composite LFs internally consistent.

5. Conclusions

We study the composite LF of 204 the SDSS CE galaxy clusters. Over all composite LF is compared with other composite LFs. Comparing it to the field luminosity function, the

tendency of brighter M^* and flatter slope is seen. This is consistent with our understanding that cluster regions are dominated by brighter galaxies than field galaxies. We divide the composite LF by galaxy morphology in three ways. In all three cases, we see early–type galaxies have flatter slopes than late–type galaxies. These observations are in agreement with the hypothesis that the bright end of the cluster LF is dominated by bright, old early–types, while the faint–end of the cluster LF represents late–type galaxies. This is also consistent with morphology-density relation originally advocated by Dressler et al. (1980, 1997). We also study these composite LFs in five SDSS color bands. The slopes become flatter and flatter toward the redder color bands. This again suggests cluster regions are dominated by elliptical galaxies with old stellar population. These composite LFs provide good low redshift benchmark to study higher redshift clusters in the future. Since data in this work come from 2% of SDSS data, further studies with large SDSS data will increase the statistical significance on these topics as the SDSS proceeds.

References

Adami, C., Ulmer, M. P., Durret, F., Nichol, R. C., Mazure, A., Holden, B. P., Romer, A. K., & Savine, C. 2000, A&A, 353, 930

Annis, J. et al. 2002 *in preparation*

Binggeli, B., Sandage, A., & Tammann, G. A. 1988, ARA&A, 26, 509

Blanton, M. R. et al. 2001, AJ, 121, 2358

Boyce, P. J., Phillipps, S., Jones, J. B., Driver, S. P., Smith, R. M., & Couch, W. J. 2001, MNRAS, 328, 277.

Colless, M. 1989, MNRAS, 237, 799

Driver, S. P., Couch, W. J., & Phillipps, S. 1998, MNRAS, 301, 369

Dressler, A. 1980, ApJ, 236, 351

Dressler, A. et al. 1997, ApJ, 490, 577

Dressler, A., Smail, I., Poggianti, B. M., Butcher, H., Couch, W. J., Ellis, R. S., & Oemler, A. J. 1999, ApJS, 122, 51

Fukugita, M., Shimasaku, K., & Ichikawa, T. 1995, PASP, 107, 945

Fukugita, M., Ichikawa, T., Gunn, J. E., Doi, M., Shimasaku, K., & Schneider, D. P. 1996, AJ, 111, 1748.

Garilli, B., Maccagni, D., & Andreon, S. 1999, A&A, 342, 408

Gladders, M. D. & Yee, H. K. C. 2000, AJ, 120, 2148

Goto, T. et al. 2002, AJ, 123, 1807.

Gunn, J.E., Carr, M., Rockosi, C., Sekiguchi, M., Berry, K., Elms, B., de Haas, E., Ivezic , Z. et al. 1998, AJ, 116, 3040 5

Hausman, M. A. & Ostriker, J. P. 1978, ApJ, 224, 320

Heydon-Dumbleton, N. H., Collins, C. A., & MacGillivray, H. T. 1989, MNRAS, 238, 379

Hogg, D.W., Finkbeiner, D.P., D.J., Gunn J.E. 2002, astro-ph/0106511

Ichikawa, S. 1986, Ann. Tokyo Astron. Obs., 21, 77

Kodama, T., Smail, I., Nakata, F., Okamura, S., & Bower, R. G. 2001, ApJL, 562, L9

Lugger, P. M. 1986, ApJ, 303, 535

Lugger, P. M. 1989, ApJ, 343, 572.

Lumsden, S. L., Nichol, R. C., Collins, C. A., & Guzzo, L. 1992, MNRAS, 258, 1

Lumsden, S. L., Collins, C. A., Nichol, R. C., Eke, V. R., Guzzo, L., 1997, MNRAS, 290, 119

Lupton, R. H., Gunn, J. E., & Szalay, A. S. 1999, AJ, 118, 1406

Lupton, R. H., Gunn, J. E., Ivezić, Z., Knapp, G. R., Kent, S., & Yasuda, N. 2001, Astronomical Data Analysis Software and Systems X, ASP Conference Proceedings, Vol. 238. Edited by F. R. Harnden, Jr., Francis A. Primini, and Harry E. Payne. San Francisco: Astronomical Society of the Pacific, ISSN: 1080-7926, 2001., p.269, 10, 269

Lupton, R. et al. 2002, *in preparation*

Okamoto, T. & Nagashima, M. 2001, ApJ, 547, 109

Paolillo, M., Andreon, S., Longo, G., Puddu, E., Gal., R. R., Scaramella R., Djorgovski, S. G., de Carvalho, R. 2001, A&A, 367, 59

Phillipps, S., Driver, S. P., Couch, W. J., & Smith, R. M. 1998, ApJL, 498, L119

Rakos, K. D., Schombert, J. M., Odell, A. P., & Steindling, S. 2000, ApJ, 540, 715

Sandage, A., Binggeli, B., & Tammann, G. A. 1985, AJ, 90, 1759

Scranton, R. et al. 2002 *in preparation*

Shimasaku, K. et al. 2001, AJ, 122, 1238

Smith, J.A., Tucker, D.L., 2002, *to appear in* AJ

Springel, V., White, S. D. M., Tormen, G., & Kauffmann, G. 2001, MNRAS, 328, 726

Strateva, I. et al. 2001, AJ, 122, 1861

Struble, M. F. & Rood, H. J. 1987, ApJ, 323, 468

Stoughton et al. 2002, accepted for AJ

Trentham, N. 1998, MNRAS, 294, 193

Valotto, C. A., Nicotra, M. A., Muriel, H., & Lambas, D. G. 1997, ApJ, 479, 90.

Valotto, C. A., Moore, B., & Lambas, D. G. 2001, ApJ, 546, 157.

Whitmore, B. C., Gilmore, D. M., & Jones, C. 1993, ApJ, 407, 489

Yagi, M., Kashikawa, N., Sekiguchi, M., Doi, M., Yasuda, N., Shimasaku, K., & Okamura, S. 2002, AJ, 123, 87.

Yagi, M., Kashikawa, N., Sekiguchi, M., Doi, M., Yasuda, N., Shimasaku, K., & Okamura, S. 2002, AJ, 123, 66.
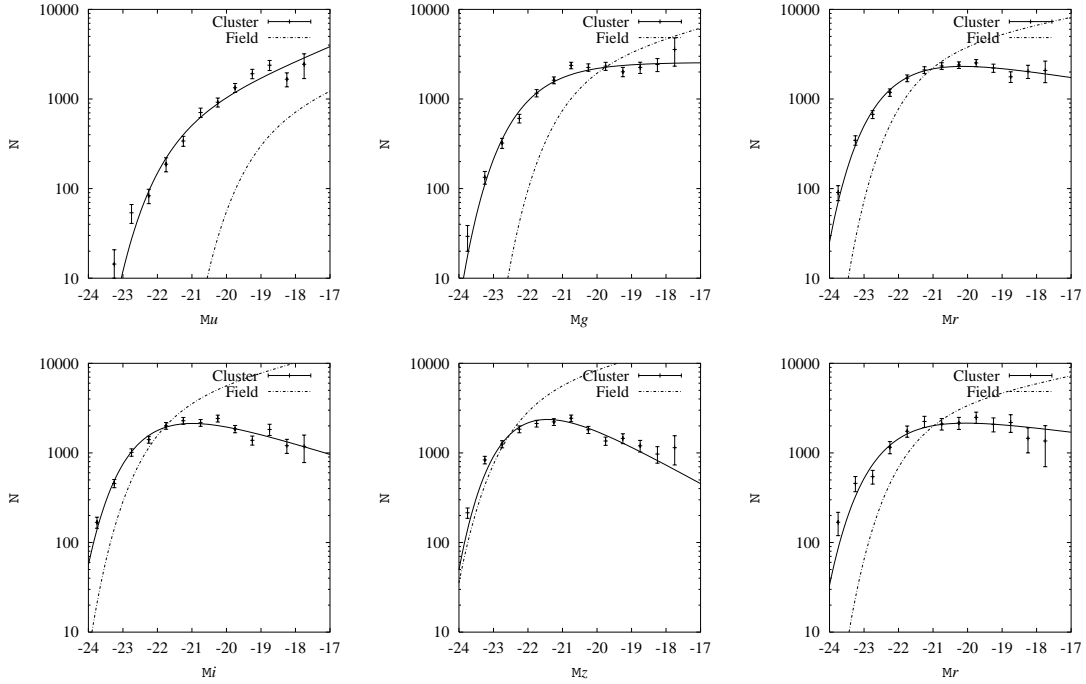
York, D. G. et al. 2000, AJ, 120, 1579

Fig. 1. Composite LF of galaxy clusters from the SDSS CE galaxy cluster catalog in five SDSS bands. The solid line is the best fit Schechter functions. Y-axis is arbitrary. The dotted line is field LFs from Blanton et al. (2001) re-scaled to our cosmology. The normalization of field LFs is adjusted to match cluster best-fit Schechter functions. The lower right panel is for clusters with spectroscopic redshifts in r^*. The best fit Schechter parameters are summarized in Table 1.

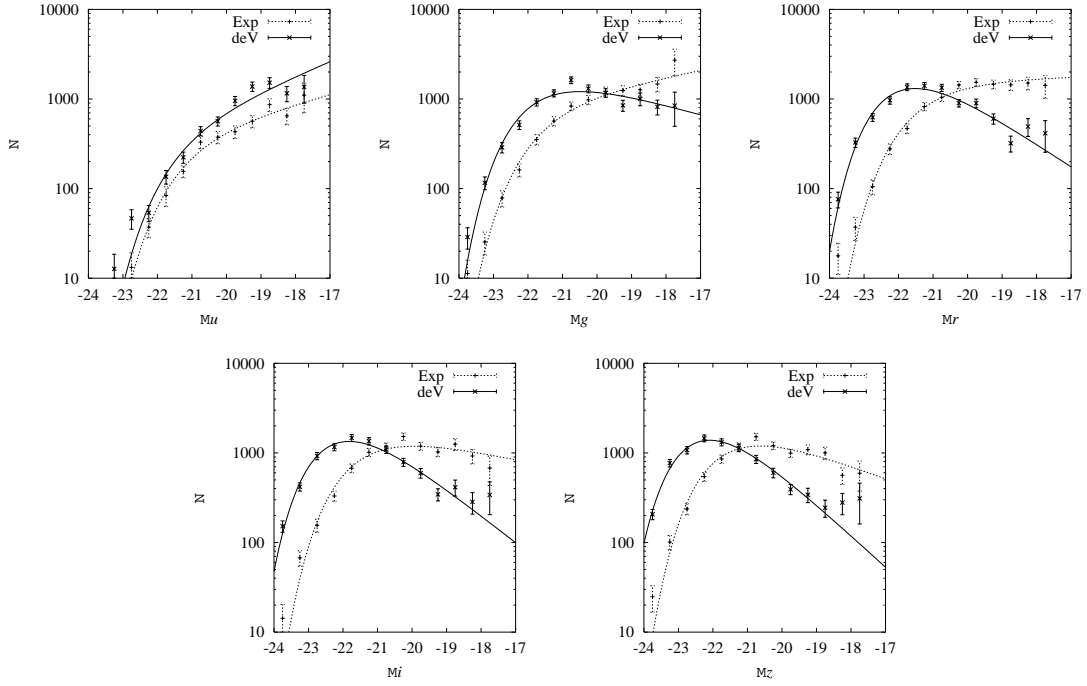**Fig. 2.** Composite luminosity functions of de Vaucouleur galaxies and exponential galaxies. Galaxies are divided into two subsamples using profile fitting. Lines show the best fit Schechter functions (solid for de Vaucouleur galaxies, dotted for exponential galaxies). Y-axis is arbitrary. de Vaucouleur galaxies always have brighter M^* and flatter faint end tail. The best fit Schechter parameters are summarized in Table 2.
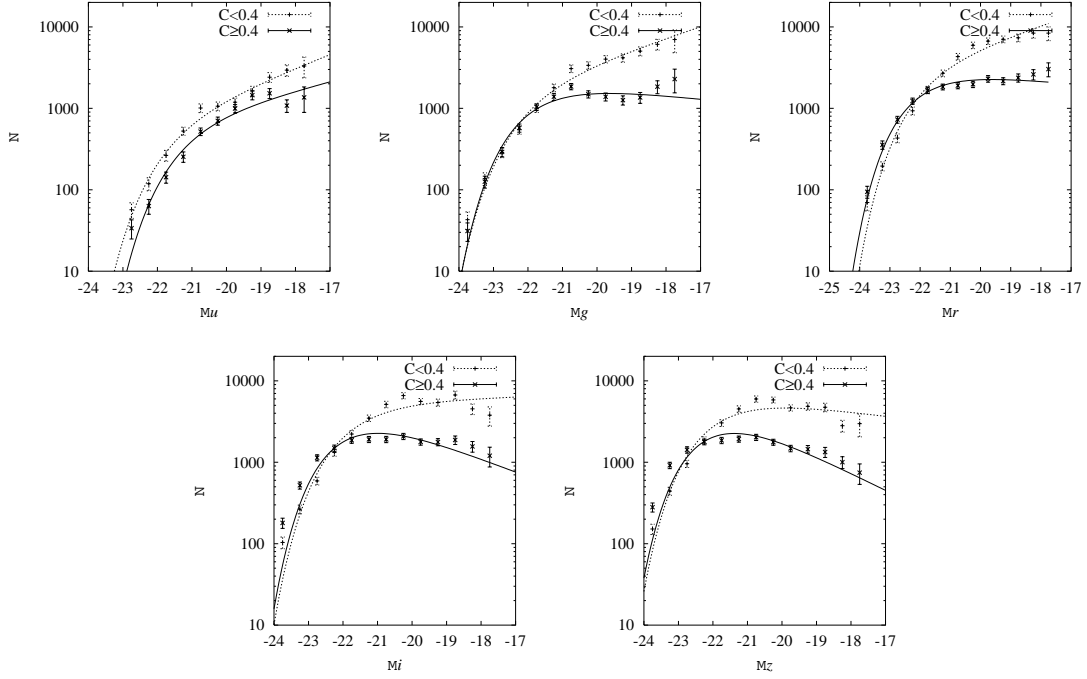
Fig. 3. Composite luminosity functions of high concentration and low concentration galaxies. The concentration index (C) used here is the ratio of 50% Petrosian flux radius to 90% Petrosian flux radius. In this figure, early–type galaxies have $C < 0.4$, late–type galaxies have $C \geq 0.4$. Early–type galaxies have flatter faint end tails in all five bands. Lines are the best fit Schechter functions (solid for $C < 0.4$, dotted for $C \geq 0.4$). Y-axis is arbitrary. The best fit Schechter parameters are summarized in Table 3.

17
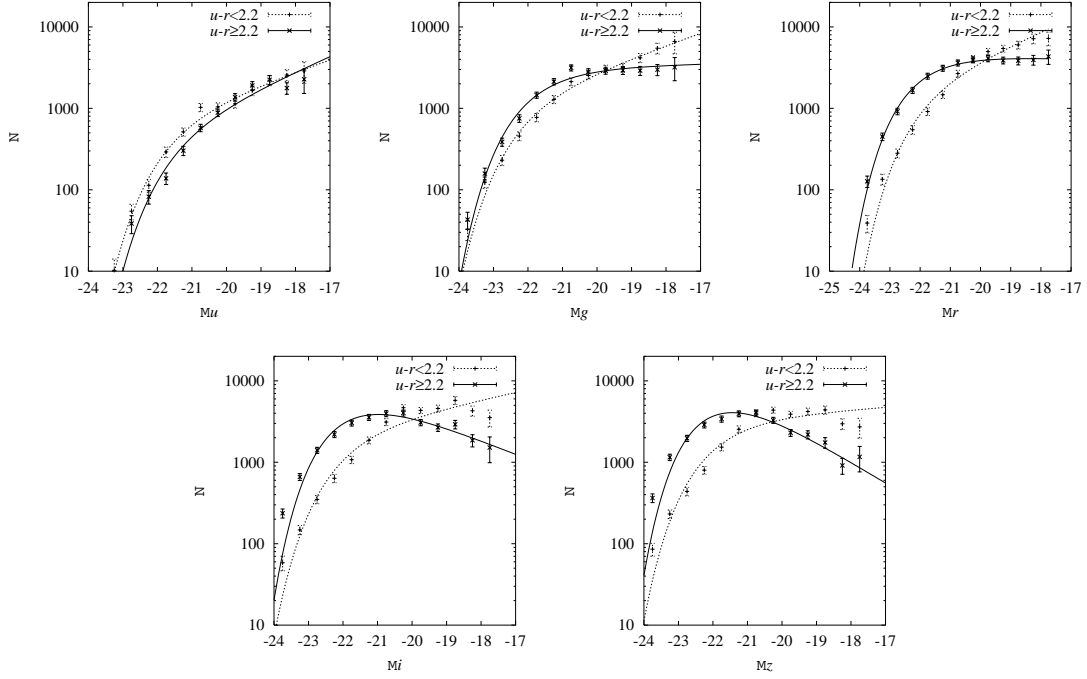
Fig. 4. Composite luminosity functions of $u^* - r^* < 2.2$ (late type) and $u^* - r^* \geq 2.2$ (early type) galaxies. Early–type galaxies have flatter faint end tails in all five bands. Lines are the best fit Schechter functions (solid for $u^* - r^* < 2.2$, dotted for $u^* - r^* \geq 2.2$). Y-axis is arbitrary. The best fit Schechter parameters are summarized in Table 4.
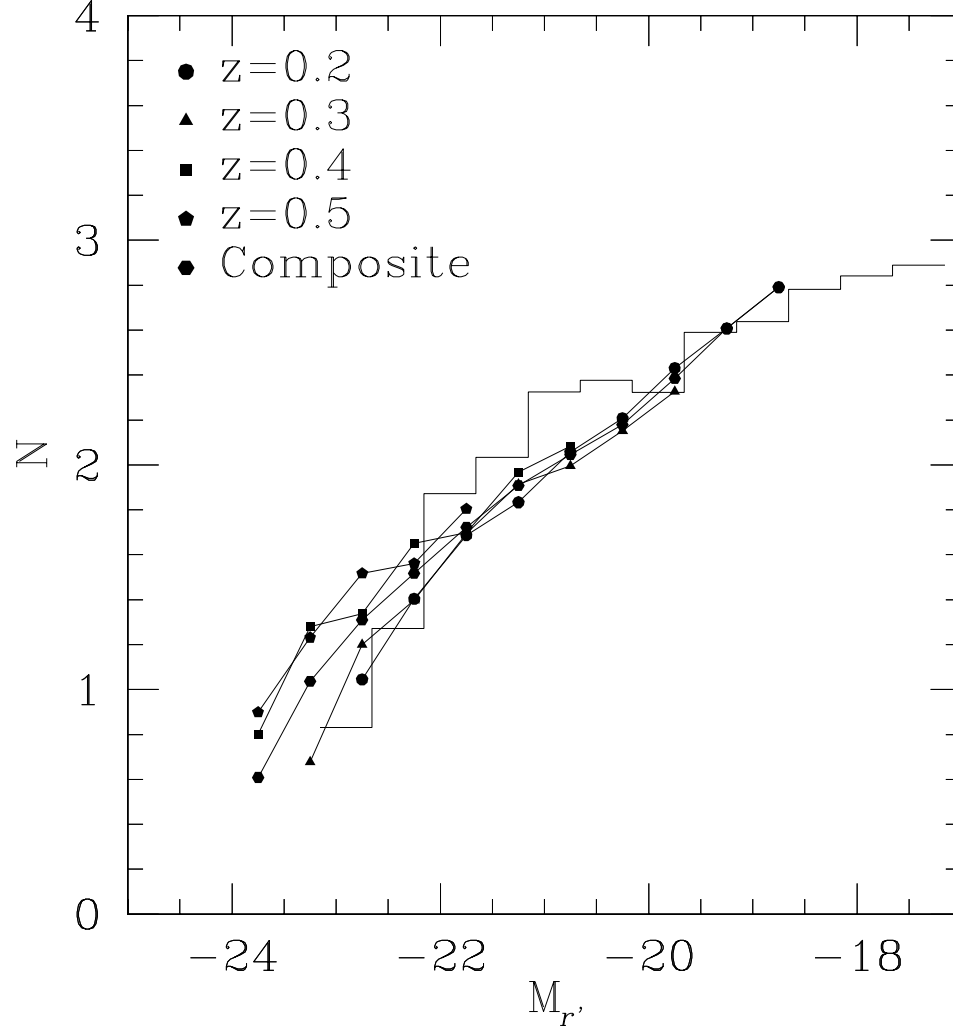
Fig. 5. Results of Monte Carlo simulation to test the robustness of the weighting scheme. The histogram shows the luminosity function of model cluster A1577. Circle, triangle, square and pentagon dots present the composite luminosity function at each redshift (z=0.2, 0.3. 0.4 and 0.5, respectively) constructed with 100 fake clusters at each redshift. Hexagonal dots show the composite luminosity function from all 400 fake clusters distributed on the real SDSS data.

Table 1. Best fit Schechter parameters of composite luminosity function of five SDSS bands. Field values are from Blanton et al. (2001), whose paramters are shifted to match our cosmology. Galaxies within 0.75 Mpc are used.

band	M^*	α	Field M^*	Field α
u^*	-21.61±0.26	-1.40±0.11	-19.11±0.08	-1.35±0.09
g^*	-22.01±0.11	-1.00±0.06	-20.81±0.04	-1.26±0.05
r^*	-22.21±0.05	-0.85±0.03	-21.60±0.03	-1.20±0.03
i^*	-22.31±0.08	-0.70±0.05	-22.03±0.04	-1.25±0.04
z^*	-22.36±0.06	-0.58±0.04	-22.32±0.05	-1.24±0.05
r^*(spec)	-22.31±0.13	-0.88±0.07	-	-

Table 2. Best fit Schechter parameters for de Vaucouleur and exponential galaxies in five SDSS bands. Galaxies are divided into two subsamples using profile fitting. Galaxies within 0.75 Mpc are used.

band	M^* (deV)	α (deV)	M^*(exp)	α (exp)
u^*	-21.64±0.30	-1.41±0.12	-21.45±0.13	-1.27±0.07
g^*	-21.92±0.11	-0.73±0.07	-21.89±0.13	-1.20±0.06
r^*	-22.01±0.07	-0.37±0.06	-21.73±0.12	-1.04±0.06
i^*	-22.13±0.07	-0.25±0.06	-21.69±0.13	-0.80±0.08
z^*	-22.24±0.06	+0.12±0.06	-21.76±0.11	-0.65±0.07

Table 3. Best fit Schechter parameters for low concentration (early–type) and high concentration (late–type) galaxies in five SDSS bands. The concentration index here is the ratio of 50% Petrosian flux radius to 90% Petrosian flux radius. Early–type galaxies have concentration<0.4, late–type galaxies have concentration≥0.4. Galaxies within 0.75 Mpc are used.

band	M^* (Early)	α (Early)	M^*(Late)	α (Late)
u^*	-21.42±0.24	-1.28±0.12	-21.82±0.11	-1.42±0.06
g^*	-22.05±0.11	-0.89±0.07	-22.26±0.11	-1.36±0.05
r^*	-22.31±0.06	-0.92±0.04	-22.24±0.12	-1.32±0.06
i^*	-21.97±0.09	-0.59±0.10	-22.02±0.13	-1.04±0.08
z^*	-22.08±0.09	-0.47±0.09	-22.09±0.12	-0.87±0.07

Table 4. Best fit Schechter parameters for $u^* - r^* > 2.2$ (early type) and $u^* - r \leq 2.2$ (late type) galaxies in five SDSS bands. Galaxies within 0.75Mpc are used.

band	M^* (Early)	α (Early)	M^* (Late)	α (Late)
u^*	-21.65±0.26	-1.47±0.11	-21.78±0.13	-1.37±0.07
g^*	-22.04±0.10	-1.03±0.06	-22.30±0.09	-1.38±0.05
r^*	-22.29±0.04	-0.97±0.02	-22.22±0.12	-1.41±0.06
i^*	-21.91±0.08	-0.58±0.07	-22.17±0.16	-1.23±0.08
z^*	-21.93±0.07	-0.36±0.08	-22.14±0.19	-1.08±0.09

Table 5. Position shuffling test of the code. Cluster declinations are randomly shuffled and the same code is applied to the shuffled clusters. Galaxies within 0.75 Mpc are used. LFs in all the bands are significantly different from the cluster LFs.

band	M^*	α
u^*	-22.28±0.27	-1.26±0.09
g^*	-22.698±0.13	-1.17±0.04
r^*	-22.65±0.18	-1.09±0.07
i^*	-22.58±0.13	-1.00±0.06
z^*	-22.55±0.11	-0.89±0.05

Table 6. Best fit Schechter parameters for galaxies using positions of brightest cluster galaxies as a center in five SDSS bands. Mean deviation from CE center used in this work is 1.02 arcmin.

band	M^*	α
u^*	-21.84±0.16	-1.43±0.07
g^*	-22.16±0.15	-1.05±0.07
r^*	-22.29±0.05	-0.91±0.03
i^*	-22.31±0.06	-0.73±0.03
z^*	-22.18±0.07	-0.55±0.07

Table 7. Best fit Schechter parameters for galaxies using global background subtraction in five SDSS bands. Instead of the annuli around the cluster, the global background is used to subtract the background galaxies to see the dependence on background subtraction.

band	M^*	α
u^*	-21.77±0.17	-1.47±0.07
g^*	-22.01±0.12	-1.06±0.07
r^*	-22.20±0.05	-0.90±0.03
i^*	-22.24±0.07	-0.72±0.04
z^*	-22.10±0.06	-0.50±0.06

Table 8. Best fit Schechter parameters in r^* band for galaxies using richer systems. Best fit Schechter parameters for $N_{-18} > 20$ and $N_{-18} > 40$ subsamples are shown. N_{-18} is defined as number of galaxies brighter than -18th magnitude after subtracting the background.

band	M^*	α	N(cluster)
$N_{-18} > 20$	-22.21±0.05	-0.85±0.03	204
$N_{-18} > 40$	-22.29±0.06	-0.90±0.04	120

Table 9. Comparison with previous works on composite luminosity function. The CE composite LFs (This work) is re-calculated using each author's cosmology. Magnitude is transformed using Fukugita et al. (1995) and Lumsden et al. (1992).

Paper	M^*	α	Band	Ncluster	Cosmology
CE	-22.21±0.05	-0.85±0.03	r^*	204	Ω_M=0.3 Ω_Λ=0.7 H$_0$=70
Colless 89	-20.04	-1.21	bj	14 rich	H$_0$=100 q$_0$=1
(CE)	-21.58±0.12	-0.93±0.06	bj	204	H$_0$=100 q$_0$=1
(CE)	-22.20±0.12	-1.21 fixed	bj	204	q$_0$=1 H$_0$=100
Lugger 89	-22.81±0.13	-1.21±0.09	R (PDS)	9	H$_0$=50
(CE)	-22.49±0.06	-0.69± 0.05	R (PDS)	204	H$_0$=50 q$_0$=0.5
(CE)	-22.77±0.17	-1.21 fixed	R (PDS)	204	H$_0$=50 q$_0$=0.5
Valotto 97	-20.0±0.1	-1.4±0.1	bj	55 Abell APM	H$_0$=100
(CE)	-21.58±0.12	-0.93±0.06	bj	204	H$_0$=100 q$_0$=1
(CE)	-22.69±0.23	-1.4 fixed	bj	204	H$_0$=100 q$_0$=1
Lumsden 97	-20.16±0.02	-1.22±0.04	bj	22 richer	q$_0$=1 H$_0$=100
(CE)	-21.58±0.12	-0.93±0.06	bj	204	q$_0$=1 H$_0$=100
(CE)	-22.22±0.10	-1.22 fixed	bj	204	q$_0$=1 H$_0$=100
Garilli 99	-22.16±0.15	-0.95±0.07	r (CCD)	65 Abell X-ray	H$_0$=50 q$_0$=0.5
(CE)	-22.15±0.06	-0.69± 0.05	r (CCD)	204	H$_0$=50 q$_0$=0.5
(CE)	-22.28±0.05	-0.84 fixed	r (CCD)	204	H$_0$=50 q$_0$=0.5
Paolillo 00	-22.26±0.16	-1.11	r (POSSII)	39 Abell	H$_0$=50 q$_0$=0.5
(CE)	-22.15±0.06	-0.69± 0.05	r (POSSII)	204	H$_0$=50 q$_0$=0.5
(CE)	-22.55±0.12	-1.11 fixed	r (POSSII)	204	H$_0$=50 q$_0$=0.5
Yagi 02	-21.3±0.2	-1.31±0.05	R_C	10 Abell	H$_0$=100 q$_0$=0.5
(CE)	-21.89±0.10	-1.03± 0.05	R_C	204	H$_0$=100 q$_0$=0.5
(CE)	-22.55±0.14	-1.31 fixed	R_C	204	H$_0$=100 q$_0$=0.5